A Synopsis of Thesis research work
(within 5000 words)
for the Degree of Doctor of Philosophy

by

Sangita Bera
(Registration No. : R-15RS09210067 dated August 12, 2016)

Supervisor: Dr. Barnali Chakrabarti

Dept.of Physics
Presidency University, College Street, Kolkata-73

PRESIDENCY UNIVERSITY
KOLKATA

A Synopsis of Thesis research work
(within 5000 words)

Thermodynamics and Statistical Fluctuations for the Trapped Interacting Bose Gas

Submitted by: Sangita Bera

Supervised by: Dr. Barnali Chakrabarti

Registration No. : R-15RS09210067 dated August 12, 2016)
Email:sangita.rs@presiuniv.ac.in/sangitaberan@gmail.com
Degree for which submitted: Doctor of Philosophy

Department of Physics
Presidency University
Kolkata-700073
India
October,2018

Dr. Barnali Chakrabarti
(Signature of the Supervisor)

Sangita Bera
(Signature of the Candidate)

I. INTRODUCTION

Bose-Einstein condensation was realized in 1995 in dilute gases of ultracold alkali bosons by three independent research groups (Ketterle at MIT, Cornell and Wieman at JILA, both for repulsive system and Hulet at Rice for attractive system) [1–3]. Since then the field of ultracold atoms has seen galloping experimental and theoretical developments. At ultracold temperature, interacting gases allow an unprecedented amount of experimental control and serve as a quantum simulator for other many-body physics which do not offer the same flexibility. Thus ultracold Bose gas and Bose-Einstein condensation represents a rich many-body system which is a challenging problem of contemporary physics and beyond the scope of mean-field Gross-Pitaevskii (GP) equation. My research interest is specially on many-body physics in connection with ultracold Bose gas and numerical investigation is done on a many-body level from first principle. Here I have studied two interrelated many-body formulation to pursue my research work. They are as follows: The first one (Correlated Potential Harmonics Expansion Method-CPHEM) solves the time-independent Schrödinger equation with two-body correlated basis function and realistic interaction and can handle quite large number bosons which mimics the JILA trap experiment; thus this approach is ideally suitable to describe statistical and thermodynamic properties. The second one (Multi Configuartional Time-Dependent Hartree for bosons-MCTDHB) solves the time-dependent N-body Schrödinger equation which in principle and by construction is exact, specially valid for finite (N is order of few tens) systems and exhibits exact many-body physics.

After the experimental realization of BEC several theoretical methods emerges to explain the results obtained. Mean-field Gross-Pitaevskii (GP) theorygross,pitaevskii, Diffusion Monte Carlo method (D-QMC) [9–11] and variational Monte Carlo (V-QMC)[12] method etc. are the very popular names to study the BEC theoretically. But GP-theory considers only contact interaction and neglect any correlation between the atoms so can give only a gross macroscopic picture of the system. Though Monte Carlo method is an exact many-body method but it can take care of only about 100 particles. To overcome these drawbacks and to have a exact many-body method, where the correlation between the atoms have been considered and a realistic interatomic potential is introduced, I will utilize correlated potential harmonics expansion method (CPHEM) [34–38]. To study the statistical fluctuations and thermodynamic properties of a trapped dilute BEC we have to consider very large number of particles and we have to solve many-body Schrödinger equation exactly. For solution I will utilize CPHEM method which is a subset of hyperspherical harmonics expansion method (HHEM) which includes all the two- and higher-body correlation [16]. But the rate of convergence is very slow when we move from particle number 3 to 4 because of the degeneracy of the basis. So for our purpose to be served we will use PHEM method which considers only two-body correlation and neglect all the higher body correlation. We experimental BEC the density is $n \sim 10^{13} - 10^{15}$ and the thermal de Broglie wavelength is comparable to $n^{-1/3}$. The interparticle separation is very large in comparison with the range of the effective potential. So for this very dilute gas three-body collision and probability of molecule formation is very small so keeping only the two-body correlation is a good approximation in the context of experimental BEC.

In this synopsis I will elaborate how to calculate different statistical and thermodynamic properties like condensate fraction, different orders of moments and specific heat of a many-body quantum system (trapped BEC) using CPHEM method. In my research work I mainly focused on the attractive and repulsive interacting BEC trapped in harmonic as well as anharmonic trap. Though for the ideal Bose gas (IG) the exact canonical recursion relation for the partition function is known and the condensate statistics and several thermodynamical properties of IG is clearly understood [13–15]. All these calculations depends on the Bogoliubov approach and are not accurate. There are some work on interacting BEC for 1D-case and also repulsive interacting BEC has been studied by our CPHEM method previously[18–23]. So in my work I will present the result for 3D-attractive and also repulsive BEC. I have studied some statistical properties like condensate fraction, fluctuation of the ground state occupation and several orders of central moments for the attractive ^7Li and repulsive ^{87}Rb system. To understand the undiscovered area of phase transition in a BEC I have studied thermodynamic quantity like specific heat for the repulsive system to give an estimate of the transition exponent.

In the later part of my study I have focused on the dynamical properties of ultracold Bose gases. To know the microscopic features of a many-body system there is no need to consider a large number of particles but a few is sufficient. We will solve time dependent Schrödinger equation to get the many body wave function. For only $N = 10$ particles the complex wave function needs a huge space for the numerical computation. To avoid this situation a clever approach to represent the high-dimensional and time-dependent many-body state of a system is considered which is MCTDHB method. MCTDHB is formulated in multiconfigurational ansatz that is a sum of all possible different configurations of N particles in M orbitals weighted by complex time-dependent coefficients [26–29]. Highly interacting and correlated system can be easily handled with this method. We can very precisely identify different states like condensation (means that all particles occupy the same single-particle state) and fragmentation (means that the particles macroscopically occupy several single particle states and is built up by taking a symmetrized product of several single particle states) of a ultracold Bose gas by measuring several quantities like density profile and occupation of different orbitals. My synopsis mainly focuses on the effect of the long range interaction specially

dipolar interaction on several properties like density distribution, energies of the a system in harmonic oscillator trap also in optical lattice. The effect of contact interaction to reach fermionization and dipolar interaction to reach crystallization and how to sort them from each other has been studied. The way how a system relaxes and approaches to thermalization can be studied through the variation of Shannon information entropy and occupation entropy. So I will give a comprehensive picture of this transition for contact interaction and also for several long range interactions for harmonic oscillator trap. To get more insight into the relaxation process we will consider a system of Bose gas in an optical lattice with periodic boundary condition and show the time evolution of entropy for two different type of quenches. For small interaction quench the system shows long time collapse-revival scenario but for large interaction quench the system relaxes to maximum entropy state. But for lattice depth quench the system shows two exactly different kind of relaxation dynamics where the system never relaxes to the maximum entropy state but shows long time collapse-revival dynamics.

II. METHODOLOGY

A. Methodology for weakly interacting many-body system :CPHEM

1. PH Basis calculation

Consider a system of $N = (A + 1)$ identical bosons, each of mass m, confined in a spherically symmetric harmonic oscillator potential of frequency ω. The N-body Schrödinger equation for the trapped atoms can be written as

$$\Big[\frac{-\hbar^2}{2m}\sum_{i=1}^{N}\nabla_i^2 + \sum_{i=1}^{N}\frac{1}{2}m\omega^2 r_i^2 + \sum_{i,j>i}^{N} V(\vec{r_i} - \vec{r_j}) - E\Big]\psi(\vec{r}_i, ..., \vec{r}_N) = 0, \tag{1}$$

where V'_{trap} is the external harmonic oscillator potential and can be written as

$$V'_{trap} = \sum_{i=1}^{N}\frac{1}{2}m\omega^2 r_i^2, \tag{2}$$

where r_i is the position vector of i-th particle from the centre of mass. Third term is the two-body interacting potential. Now we introduce A number of Jacobi vectors as

$$\vec{\zeta_i} = \sqrt{\frac{2i}{i+1}}\left(\vec{r}_{i+1} - \frac{1}{i}\sum_{j=1}^{i}\vec{r}_j\right), \qquad (i = 1, ..., A). \tag{3}$$

By using these Jacobi vectors we can separate out the N-body Schrödinger equation in centre of mass motion and relative motion. The Schrödinger equation for the relative motion is

$$\Big[\frac{-\hbar^2}{m}\sum_{i=1}^{A}\nabla_{\vec{\zeta}_i}^2 + V_{trap} + \sum_{i,j>i}^{A} V(\vec{\zeta_i} - \vec{\zeta_A}) - E_R\Big]\psi(\vec{\zeta}_1, ..., \vec{\zeta}_A) = 0, \tag{4}$$

where E_R is the energy of the relative motion and

$$V_{trap} = \sum_{i=1}^{A}\frac{1}{2}m\omega^2\zeta_i^2. \tag{5}$$

The evolution of the system can be viewed by following the motion of one point in $3A$-dimensional hyperspace. The polar coordinates of this point are expressed by the hyperspherical variables. In our method we consider that when any (ij) pair of atoms are interacting then all the other particles are just inert spectators because we are dealing

with very dilute BEC so all the higher-body interactions can be ignored and the wave function ψ can be expanded in two-body Faddeev component (ϕ_{ij}) which is a function of only r_{ij}. This ϕ_{ij} can be expanded as

$$\phi_{ij}(\vec{r}_{ij}, r) = r^{-\frac{(3A-1)}{2}} \sum_K \mathcal{P}^{lm}_{2K+l}(\Omega^{ij}_A) u^l_K(r). \tag{6}$$

Where Ω^{ij}_A denotes the full set of hyperangles in the 3A dimensional space corresponding to the (ij)-th interacting pair and $\mathcal{P}^{lm}_{2K+l}(\Omega^{ij}_A)$ is called potential harmonic (PH) basis. The hyperradius is defined as

$$r = \left[\sum_{i=1}^{A} \zeta_i^2\right]^{\frac{1}{2}}. \tag{7}$$

So the hyperradius for the $(A-2)$ particles can be written as

$$\rho_{ij} = \Big[\sum_{i=1}^{A-1} \zeta_{ij}^2\Big]^{1/2}, \tag{8}$$

so that

$$r^2 = r_{ij}^2 + \rho_{ij}^2 \tag{9}$$

where $\vec{r}_{ij}$ is the relative vector of the $(i-j)$ pair of particles. The hyperangle ϕ is introduced as $r_{ij} = r\cos\phi$ and $\rho_{ij} = r\sin\phi$. Besides r,ϕ,φ and ϑ there are $(3A-4)$ remaining variables. These are constituted by $2(A-1)$ polar angles associated with $(A-1)$ Jacobi vectors $(\vec{\zeta_1}, ...\vec{\zeta_{A-1}})$ and $(A-2)$ angles defining their relative lengths and collectively denoted by $\Omega^{ij}_{(A-1)}$ called hyperangles in the $3(A-1)$-dimensional space. The corresponding form of Laplace operator is given in the reference [16].

Substitution of Eq.(6) into the Schrödinger equation we finally get a coupled differential equation as

$$\begin{aligned}\Big[&-\frac{\hbar^2}{m}\frac{d^2}{dr^2} + \frac{\hbar^2}{mr^2}\{\mathcal{L}(\mathcal{L}+1) + 4K(K+\alpha+\beta+1)\} \\ &+ V_{trap}(r) - E_R\Big] U_{Kl}(r) \\ &+ \sum_{K'} f_{Kl} V_{KK'}(r) f_{K'l} U_{K'l}(r) = 0,\end{aligned} \tag{10}$$

where $U_{Kl}(r) = f_{Kl}\ u^l_K(r)$, $\mathcal{L} = l + \frac{3N-6}{2}$, $\alpha = \frac{3N-8}{2}$, $\beta = l + \frac{1}{2}$, l being the orbital angular momentum of the system contributed by the interacting pair and and K is called the grand orbital quantum number. f_{Kl} is a constant and represents the overlap of the PH for interacting pair of particles with the sum of PHs corresponding to all pairs [17] and given by

$$f^2_{Kl} = \sum_{k,l>k} <P^{lm}_{2K+l}(\Omega^{ij}_A) \mid P^{lm}_{2K+l}(\Omega^{kl}_A)>. \tag{11}$$

Details prescription of the methodology was discussed in our earlier works [34–38]. Resulting potential matrix element $V_{KK'}(r)$ is given by

$$V_{KK'}(r) = \int \mathcal{P}^{lm'}_{2K+l}(\Omega^{ij}_A) V(r_{ij}) \mathcal{P}^{lm}_{2K'+l}(\Omega^{ij}_A) d\Omega^{ij}_A. \tag{12}$$

To improve the rate of convergence greatly we will include a short-range correlation function $\eta(r_{ij})$. To get $\eta(r_{ij})$, we solve the two-body Schrödinger equation at zero energy to get a_s as

$$-\frac{\hbar^2}{m}\frac{1}{r_{ij}^2}\frac{d}{dr_{ij}}\left(r_{ij}^2\frac{d\eta(r_{ij})}{dr_{ij}}\right) + V(r_{ij})\eta(r_{ij}) = 0. \tag{13}$$

The asymptotic part of $\eta(r_{ij})$ has the form $c_1 r_{ij} + c_2$ and the corresponding s-wave scattering length is $a_s = -\frac{c_2}{c_1}$. For fixed C_6 value (for ^7Li or ^{87}Rb atom), we adjust the hard core radius r_c, such that a_s has the desired value. $\eta(r_{ij})$ is further used in the Eq.(6) to get the new basis as

$$\phi_{ij}(\vec{r}_{ij}, r) = r^{-\frac{(3A-1)}{2}} \sum_K \mathcal{P}^{lm}_{2K+l}(\Omega^{ij}_A) u^l_K(r)\eta(r_{ij}). \tag{14}$$

and we call it correlated PH basis (CPH).

Thus $\eta(r_{ij})$ correctly reproduces the correct short range separation of the interacting pair and offers fast convergence in the PH basis. Instead of using Eq.(12) the potential matrix is further calculated by using the equation

$$V_{KK'}(r) = (h_K^{\alpha\beta} h_{K'}^{\alpha\beta})^{-\frac{1}{2}} \int_{-1}^{+1} \left\{ P_K^{\alpha\beta}(z) V\left(r\sqrt{\frac{1+z}{2}}\right) P_{K'}^{\alpha\beta}(z) \eta\left(r\sqrt{\frac{1+z}{2}}\right) W_l(z) \right\} dz \tag{15}$$

where $z = \cos(2\phi)$, $h_K^{\alpha\beta}$ and $W_l(z)$ are respectively the norm and the weight function of the Jacobi polynomial $P_K^{\alpha\beta}(z)$ [42]. By substituting this interaction potential term along with the CPHEM basis in the Eq.(10) we can solve the final coupled differential equation by our numerical method.

2. *Requirement of the proper recursion relation to calculate partition function*

For the present study we start from the canonical ensemble which takes care of the intermediate situation of the microcanonical ensemble and the grand canonical ensemble and most appealing one. In the microcanonical ensemble the gas is completely isolated and there is no exchange of energy or atoms so it gives some over-estimated values for several statistical properties. Whereas in the grand-canonical ensemble, only the average energy per atom and the average number of atoms are fixed, thus there is an exchange of both energy and atoms which leads to the grand canonical catastrophe [45].

Landsberg first proposed a recursion method [43] to calculate the partition function of the canonical ensemble with moderate atom numbers and an iteration procedure with respect to the number of particles was used. Later Landsberg's method was improved by E. D. Trifonov *et al.* [44] to facilitate its application for larger number of particles and wider temperature range. It also demonstrated the efficiency of recursion technique for three dimensional isotropic trapped ideal Bose gas. For completeness here we briefly summaries the method which we utilize in our numerical calculation.

The probability of the N-particle system in a state, described by an occupation number $\{n_i\}$, is given by

$$P_{\{n_i\}} = \frac{1}{Z_N} \exp\left(-\frac{E_{\{n_i\}}}{k_B T}\right), \tag{16}$$

where Z_N is the partition function of the N-particle system and can be defined as,

$$Z_N = \sum_{\{n_i\}} \exp\left(-\frac{E_{\{n_i\}}}{k_B T}\right) \tag{17}$$

with the summation performed over all combinations of the occupation numbers that satisfy the condition

$$\sum_i n_i = N. \tag{18}$$

Thus the probability of finding n_k particles in k-th single particle state is determined as

$$P_{n_k}^{(k)} = \frac{Z_{N-n_k}^{(k)}}{Z_N} \exp\left(-\frac{n_k E_k}{k_B T}\right). \tag{19}$$

where $Z_{N-n_k}^{(k)}$ is the partition function for $(N - n_k)$ particles, with the k-th single-particle state excluded from the sum. E_k is the energy of the k-th single particle state.

In terms of Landsberg's recursion method using iteration with respect to the number of particles the partition function can be calculated by a simple algorithm [44] as

$$Z_n = \frac{1}{n} \sum_{p=1}^{n} S_p Z_{n-p},\ Z_0 = 1;\ n = 1, 2, ..., N \tag{20}$$

where,

$$S_p = \sum_j \exp(-\frac{pE_j}{k_B T}). \tag{21}$$

This is an ideal method where the summation can be performed analytically like three dimensional isotropic harmonic trap. Landsberg method was used to calculate the partition function of Bose gas with moderate particle number (~ 100) and for sufficiently low temperature $T << T_c$ [43]. Later Trifonov *et al.* improved the methodology for larger particle number and increasing temperature[44]. The recursion formulas are:

$$Z_0^{\{0\}} = 1 \ , \tag{22}$$

$$Z_n^{\{n-1\}} = \sum_{p=0}^{n-1} \frac{S_{n-p} Z_p^{\{n-1\}}}{n}, \ \ n = 1, ..., N, \tag{23}$$

$$Z_k^{\{n\}} = \frac{Z_k^{\{n-1\}}}{\sum_{p=0}^{n} Z_p^{\{n-1\}}}, \ \ k = 0, ..., n. \tag{24}$$

The probability of finding n_0 particles out of total particle N in the ground state is

$$P_{n_0} = Z_{N-n_0}^{\{N\}}, \tag{25}$$

where

$$Z_N = Z_N^{\{N\}} \Pi_{n=1}^{N} \sum_{p=0}^{n} Z_p^{\{n-1\}}. \tag{26}$$

The relation between the probability distribution of n_0 number of atoms in the ground states P_{n_0} and the canonical partition function is given by

$$P_{n_0} = \frac{Z_{N-n_0}(T) - Z_{N-n_0-1}(T)}{Z_N(T)} \tag{27}$$

Accordingly the mean number of particles in the ground state and its root-mean-square fluctuation can be found from the relation

$$< n_0 >= \sum_{n_0=0}^{N} n_0 P_{n_0} \tag{28}$$

and

$$\delta n_0 = \sqrt{< n_0^2 > - < n_0 >^2} \tag{29}$$

where

$$< n_0^2 >= \sum_{n_0=0}^{N} n_0^2 P_{n_0}. \tag{30}$$

The central moments are then obtained as

$$< \Big(n_0 - < n_0 > \Big)^m >= \sum_{n_0=0}^{N} \Big(n_0 - < n_0 > \Big)^m P_{n_0}. \tag{31}$$

The moment for $m = 2$ is termed as standard deviation and $m = 3, 4$ are termed as third order and fourth order central moment respectively.

B. Mehodology for strongly correlated many-body system:MCTDHB

1. Hamiltonian and numerical method

In order to discuss crystalline and fermionized bosons, we consider the time-dependent many-body Schrödinger equation,

$$i\partial_t|\Psi\rangle = \hat{H}|\Psi\rangle. \tag{32}$$

Here, $|\Psi\rangle$ is the many-body state and the N-particle Hamiltonian $\hat{H}$ in dimensionless units [46] reads,

$$H = \sum_{i=1}^{N}\left(\frac{1}{2}\frac{\partial^2}{\partial x_i^2} + V(x_i)\right) + \sum_{i<j} W(x_i - x_j), \tag{33}$$

where we set $V(x_i) = \frac{1}{2}x_i^2$ to be the external harmonic trap and $V(x_i) = V_{OL}\sin^2(kx_i)$ for optical lattice with V_{OL} as the depth of the potential. $W(x_i - x_j)$ the interaction potential. All quantities are dimensionless and expressed in harmonic oscillator units. For contact interactions

$$W(x_i - x_j) = \lambda\delta(x_i - x_j), \tag{34}$$

where λ is the interaction strength determined by the scattering length a_s and the transverse confinement frequencies [47]. For long-ranged dipolar interactions

$$W(x_i - x_j) = \frac{g_d}{|x_i - x_j|^\alpha + \alpha_0}, \tag{35}$$

where g_d is the dipolar interaction strength and α_0 is a short-range cut-off to avoid the divergence at $x_i = x_j$. By varying this α value we can change the order of the long range and for $\alpha = 3$ we have dipolar interaction. For the first part I restrict to $N = 4$ interacting bosons for all our calculations and consider repulsive interactions, $\lambda > 0$ and $g_d > 0$, exclusively. To investigate the stationary properties of the system, we propagate the wavefunction in imaginary time using the MCTDHX software [26–29] to solve the MCTDHB equations of motion [24, 25]; thereby the system relaxes to the ground state.

The computation of the exact many-body wave function is a difficult problem. To attack the time-dependent many-body Schrödinger equation, Eq. (32), we expand the many-body wavefunction $|\Psi\rangle$ of N interacting bosons in a complete set of time-dependent permanents $|\vec{n};t\rangle = |n_1,...,n_M;t\rangle$ with at most M single-particle states or orbitals. The MCTDHB ansatz for the many-body wave function is thus

$$|\Psi(t)\rangle = \sum_{\vec{n}} C_{\vec{n}}(t)|\vec{n};t\rangle. \tag{36}$$

Here, the permanents $|\vec{n};t\rangle$ are symmetrized bosonic many-body states that are also referred to as "configurations". The sum in Eq. (36) runs on all configurations $\vec{n}$ of N particles in M orbitals. The number of permanents and coefficients $C_{\vec{n}}(t)$ is $N_{conf}= \begin{pmatrix} N+M-1 \\ N \end{pmatrix}$. In the second quantized representation the permanents are given as

$$|\bar{n};t\rangle = |n_1,...n_M;t\rangle = \prod_{i=1}^{M}\left(\frac{\left(\hat{b}_i^\dagger(t)\right)^{n_i}}{\sqrt{n_i!}}\right)|vac\rangle. \tag{37}$$

Here $\hat{b}_k^\dagger(t)$ is the bosonic creation operator which creates a boson in the time-dependent single particle state $\phi_k(\vec{r},t)$. Eq. (36) spans the full N-body Hilbert space in the limit of $M\to\infty$. For practical computations, we restrict the number of orbitals and require the convergence of our observables, like the one- and two-body density matrix, with respect to the number of single-particle states M. A set of coupled equations of motion for, both, the time-dependent expansion coefficients $C_{\vec{n}}(t)$ and the time-dependent orbitals $\phi_k(\vec{r},t)$ are obtained by requiring the stationarity of the action of the time-dependent Schrödinger equation [24, 25] under variations of $C_{\vec{n}}(t)$ and $\phi_k(\vec{r},t)$. Using MCTDHB, both, the coefficients and orbitals are variationally optimized [30]. MCTDHB is thus fundamentally different from exact diagonalization, i.e., an ansatz built with *time-independent* orbitals. The set of coupled equations are solved simultaneously for the ground state using imaginary time propagation [26–29].

C. Quantities of interest

In this section, we define the quantities that we analyze in our subsequent simulations. From the many-body wave function $\psi(x_1, x_2, ...x_N; t)$, the reduced one-body density matrix (RDM) $\rho^{(1)}$ is calculated as

$$\rho^{(1)}(x'|x;t) = N \int dx_2 dx_3 ... dx_N \psi^*(x', x_2, \ldots, x_N; t) \psi^*(x, x_2, \ldots, x_N; t). \tag{38}$$

Its diagonal gives the one-body density $\rho(x,t)$ obtained as

$$\rho(x,t) = \int dx_2 dx_3 ... dx_N \psi^*(x, x_2, \ldots, x_N; t) \psi(x, x_2, \ldots, x_N; t) \tag{39}$$

and gives the probability of a particle at the position x at time t when the contribution of other particles are traced out. The non-local correlations are determined by the off-diagonal kernel of $\rho^{(1)}(x'|x;t)$. When $|x - x'| \to \infty$, the off-diagonal behavior of $\rho^{(1)}(x', x)$ measures the coherence.
The second order reduced density matrix is defined as

$$\rho^{(2)}(x_1', x_2'|x_1, x_2; t) = N(N-1) \int dx_3 dx_4 .... dx_N \psi^*(x_1', x_2', x_3, ..., x_N; t) \psi(x_1, x_2, ...x_N; t) \tag{40}$$

Its diagonal kernel is given by

$$\rho^{(2)}(x_1, x_2; t) \equiv \rho^{(2)}(x_1' = x_1, x_2' = x_2|x_1, x_2; t) \tag{41}$$

and represents the simultaneous probability of finding a boson at x_1 and another at x_2.
The Shannon information entropy (SIE) of the one-body density in position space is defined as $S_x(t) = -\int dx \rho(x,t) ln[\rho(x,t)]$ and similarly in the momentum space as $S_k(t) = -\int dk \rho(k,t) ln[\rho(k,t)]$. The two SIE as defined above are two independent key quantities in the calculation of quantum information in many-body system. The SIE is a measure of the delocalization of the corresponding distribution. However since SIE is based on the one-body density, one can not infer the presence of correlation in the many-body state. Whereas in MCTDHB, as the many-body wave function is expanded in the time-dependent coefficients as well as time-dependent orbitals, we therefore provide alternative definitions of SIE. The SIE defined from the coefficients $C_{\bar{n}}$ is called information entropy or coefficient entropy and it is calculated from

$$S^{info}(t) = -\sum_{\bar{n}} |C_{\bar{n}}(t)|^2 \ln |C_{\bar{n}}(t)|^2 \tag{42}$$

S^{info} characterizes the distribution of the many-body state in the underlying Fock-space. The many-body measure of information entropy can be explicitly made by writing the coefficients as an expectation values in terms of M creation and annihilation operator [31].

We measure the SIE related to occupation of multiple orbitals, *i.e.*, when have multiple orbitals have significant population. This is characterized by the contribution from multiple significant eigenvalues n_i; $i = 1, 2...M$ of the reduced one-body density matrix, which are also referred to as natural occupations. Thus we term it as occupation entropy and is calculated as

$$S^{occu}(t) = -\sum_{i=1}^{M} \bar{n}_i(t) \ln \bar{n}_i(t) \tag{43}$$

For the single-orbital mean-field theory, in presence of true condensation and off-diagonal long-range order [32], the reduced density matrix has only a single eigenvalue macroscopically larger than the others and S^{occu} is always zero, whereas for multiorbital mean-field theory S^{occu} remains constant. Thus the proximity of the value of S^{occu} to 0 gives again an indication of how well the state can be described by a mean-field approach.
We are also interested in the calculation of first- and second-order Glauber's normalized correlation function at many-body level which may provide additional tools to study the pathway from localization to delocalization. We will see

in the result section how these correlation functions effectively describe the crossover to GOE in terms of the loss of first-order coherence and emergence of anti-bunching effect in the second-order coherence. The normalized *pth* order correlation function is defined by

$$g^{(p)}(x'_1,...,x'_p,x_1,...,x_p) = \frac{\rho^{(p)}(x_1,...,x_p|x'_1,...,x'_p)}{\sqrt{\prod_{i=1}^{p}\rho^{(1)}(x_i|x_i)\rho^{(1)}(x'_i|x'_i)}} \tag{44}$$

and is the key quantity to define spatial p-th order coherence. Here, $\rho^{(p)}(x_1,...,x_p|x'_1,...,x'_p;t)$ is the p-th order reduced density matrix of the state $|\Psi\rangle$ [48]. In the case of $|g^{(p)}(x_1...,x_p,x_1...,x_p;t)| > 1$ (< 1), the detection probabilities of p particles at positions $x_1,...,x_p$ are referred to as (anti-)correlated.

III. THE AIM OF THE THESIS AND ITS ACHIEVEMENTS IN THAT PERSPECTIVE: SUMMARY OF RESEARCH WORK:

A. Result for weakly interacting BEC

1. *Choice of the systems and numerical results*

I have extensively studied attractive as well as repulsive interacting BEC. First I have considered N number of ^7Li atoms in a harmonic oscillator potential with oscillator frequencies $\nu_x = 150.6$ Hz, $\nu_y = 152.6$ Hz and $\nu_z = 131.5$ Hz. For our numerical calculation we will consider the oscillator frequency as $\nu = (\nu_x\nu_y\nu_z)^{\frac{1}{3}}$ which is given by $\nu = 144.944$ Hz [34]. Here all the length parameters are measured in oscillator unit of length (o.u of length) as

$$a_{ho} = \sqrt{\frac{\hbar}{m\omega}}, \tag{45}$$

where $\omega = 2\pi\nu$ and the energies are expressed in units of oscillator energy $\hbar\omega$ (o.u of energy). The interaction potential has a short range hard core of cut-off radius r_c with long range van der Waals tail

$$\begin{aligned} V(r_{ij}) &= \infty \qquad \text{for } r_{ij} < r_c \\ &= -\frac{C_6}{{r_{ij}}^6} \qquad \text{for } r_{ij} \geq r_c. \end{aligned} \tag{46}$$

We solve the two-body Schrödinger equation at zero energy and find r_c such that it reproduces the desired scattering length a_s. The value of $C_6 = 1.71487 \times 10^{-12} o.u.$ for ^7Li atoms [35]. The value of $a_s = -27.3$ corresponding to $r_c = 5.3378 \times 10^{-4} o.u$ is kept constant for our calculation and we vary the particle number N. For the second case I have chosen repulsive interacting ^{87}Rb atoms with $C_6 = 6.4898 \times 10^{-11}$ o.u, the desired scattering length is $a_s = 100$ Bohr $= 0.00433$ o.u and $r_c = 1.121 \times 10^{-3}$ o.u [39]. All our chosen parameters mimic the experiment of JILA trap [4].

We solve Eq.(10) by hyperspherical adiabatic approximation method (HAA) [40]. In HAA, hyperradial motion is adiabatically separated from the hyperangular motion. The hyperangular motion is first solved by diagonalizing the potential matrix together with hypercentrifugal repulsion for fixed value of r. The lowest eigenvalue $\Big(\omega_0(r)\Big)$ is called as the lowest eigenpotential and is used to solve the hyperradial equation

$$\Big[-\frac{\hbar^2}{m}\frac{d^2}{dr^2} + \omega_0(r) - E_R\Big]\zeta_0(r) = 0. \tag{47}$$

The whole condensate moves as a single quantum entity within $\omega_0(r)$. The plot of $\omega_0(r)$ is shown in Fig. 1(a) and 1(b). Note that the deep negative well in the left hand side corresponds to cluster and I will not study this situation here. The shallow well in the right hand side basically holds the metastable BEC and we solve it to get the full energy spectrum. We first calculate E_{nl} with $l = 0$ and $n = 0, 1, 2, ...$ values. Similarly energy levels for $l > 0$ can be calculated as hyperradial excitations in the metastable region of the effective eigenpotential. Note that for a fixed l the number of levels (maximum n, denoted by n_{max}) is fixed in the metastable region. However the maximum value of l depends on the choice of particle number N. For $N = 500$, $l_{max} = 426$ and for $N = 1300$, $l_{max} = 68$ available for the convergence in the ground state probability distribution for different temperature.

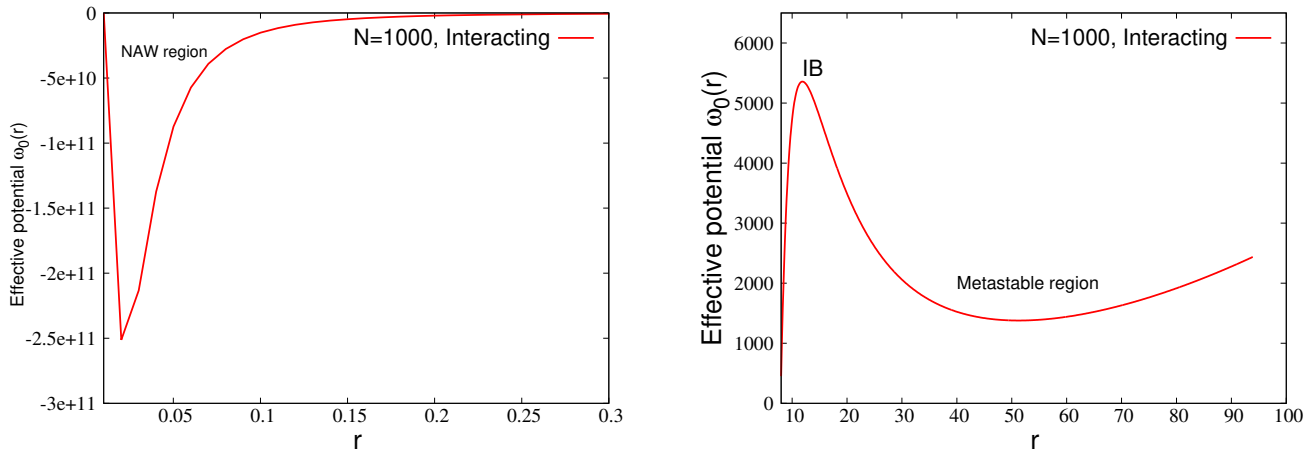

FIG. 1. Plot of effective potential for interacting bosons with N = 1000, in the harmonic trap where left panel is the narrow attractive well and right one shows the metastable region for the ^7Li condensate.

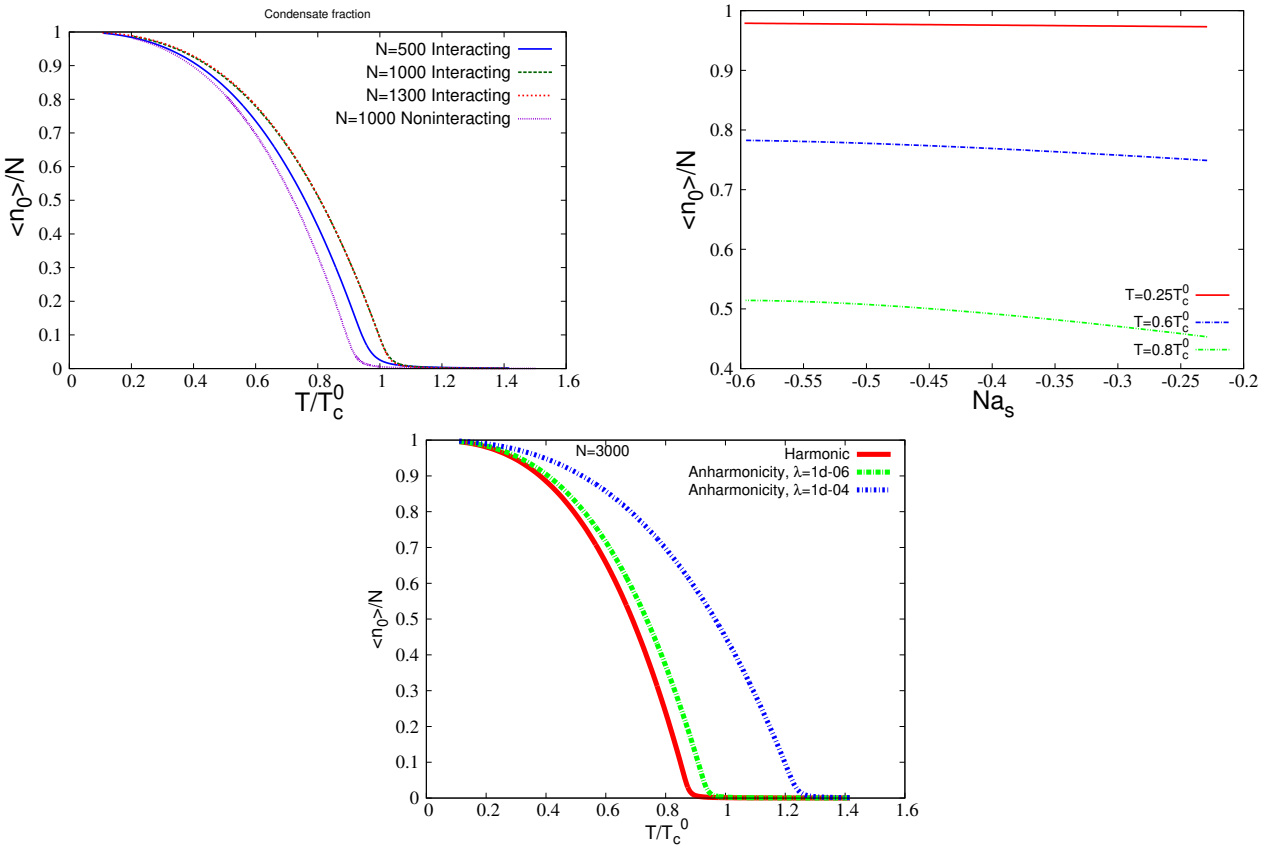

FIG. 2. Plot of $< n_0 > /N$ with respect to reduced temperature $\frac{T}{T_c^0}$ and also with the strength of the interaction (Na_s).

2. *Result for several statistical properties and condensate fluctuation*

With the help of CDE we can calculate excitation spectrum of the N particle system and also using the recursion relations for the partition function I have calculated condensate fraction, ground state probability distribution, fluctuation in the gound state population and several order of central moments.
In Fig. 2(a), we plot the condensate fraction as a function of reduced temperature for $N = 500, 1000$ and 1300 atoms. The result for ideal Bose gas is also presented for comparison. We observe that the condensate fraction exhibits

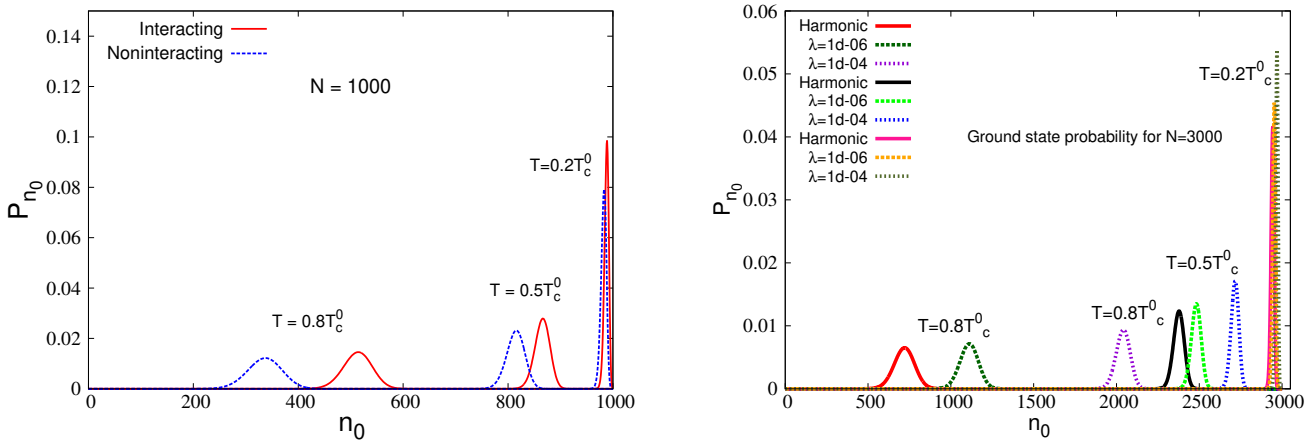

FIG. 3. (Left panel) Plot of ground state probability P_{n_0} against n_0 for interacting and noninteracting bosons with N = 1000 considering ^7Li atoms in the harmonic trap. (Right panel) The same for interacting and noninteracting bosons with N = 3000 considering ^{87}Rb atoms in the harmonic and also in anharmonic trap

smooth transition near the critical point. Although all the curves are smooth for the finite systems, the change in condensate fraction is more pronounced near the critical point due to the increase in the particle numbers. In Fig. 2(b) I have studied the variation of the condensate fraction with the strength of the interaction. It is to be noted that for the attractive condensate, with increase in total negative interaction strength parameter the local density increases with respect to the ideal gas. Naturally the number of condensate atoms shows a monotonic increasing behaviour as we move from $Na_s = 0$ (noninteracting limit) to large negative value of Na_s. Also I have studied the effect of trap geometry on the condensate fraction for repulsive interacting BEC by fixing the number of particles to $N = 3000$ and varrying the anharmonicity (λ). To do comparison the result for harmonic trap is also presented. From the Fig. 2(c), one can see that with the increase in λ for a fixed temperature T the condensate fraction increases i.e, population in the ground state increases with anharmonicity λ [41].

In Fig. 3(a) and 3(b) I have plotted the ground state probability distribution (P_{n_0}) against the temperature and also with the interaction both for the ^7Li and ^{87}Rb systems respectively. The peak values for interacting case is larger and centered at a higher value of n_0 than the non-interacting case. So we can say that attractive interaction enhances the condensation process. In Fig. 3(b) the variation of P_{n_0} is shown for harmonic and anharmonic trapped systems for three different temperature regimes, viz., $T = 0.2T_c$, $0.5T_c$, $0.8T_c$. For the repulsive Bose gas, the peak value of P_{n_0} decreases as T increases. Due to interatomic repulsion, as T increases, more and more atoms are pushed up into higher states and the ground states starts to be depleted. At $T = 0.2T_c$, the distribution shows a sharp peak near $< \bar{n}_0 >$, the distribution starts to broaden as T increases. The peak value in P_{n_0} is higher in anharmonic trap, which enhances the population in the ground state. It is also in good agreement that anharmonic trap favours BEC [15]. However the additional observation in our present calculation is at higher temperature the distributions are separably visible for harmonic and anharmonic trap with different anharmonicity. However as temperature decrease gradually the difference in the probability distribution starts to decrease and finally they almost overlap with each other.

Figure 4(a) to 4(c) describe the dependence of the root mean square fluctuation in the ground state occupation δn_0 on the number of particles, temperature and the strength of the interaction respectively. In Figure 4(a), we present the analysis of thermal fluctuation of the condensate. We plot the root-mean-square fluctuation δn_0 as a function of reduced temperature $\frac{T}{T_c^0}$. It is to be noted that for uniform and homogeneous gas (a trapless gas), the thermal fluctuation may destabilize the condensate, however the presence of harmonic confinement exhibits the BEC at finite temperature for finite size systems. It is also interesting to see the dependence of δn_0 on $\frac{k_BT}{\hbar\omega}$. In Figure 4(b), we plot δn_0 as a function of $\frac{k_BT}{\hbar\omega}$ for $N = 500, 1000$ and 1300. The curve for the ideal Bose gas in thermodynamic limit is also ploted here. We obtain this graph by utilizing the following equation [**?**]

$$< \delta^2 n_0 >= \Big(\frac{k_BT}{\hbar\omega}\Big)^3 \zeta(2) + \Big(\frac{k_BT}{\hbar\omega}\Big)^2 \Big[\frac{3}{2} ln(\frac{k_BT}{\hbar\omega}) + \frac{3}{2}\gamma + \frac{5}{4} + \zeta(2)\Big] - \frac{1}{2}\Big(\frac{k_BT}{\hbar\omega}\Big), \tag{48}$$

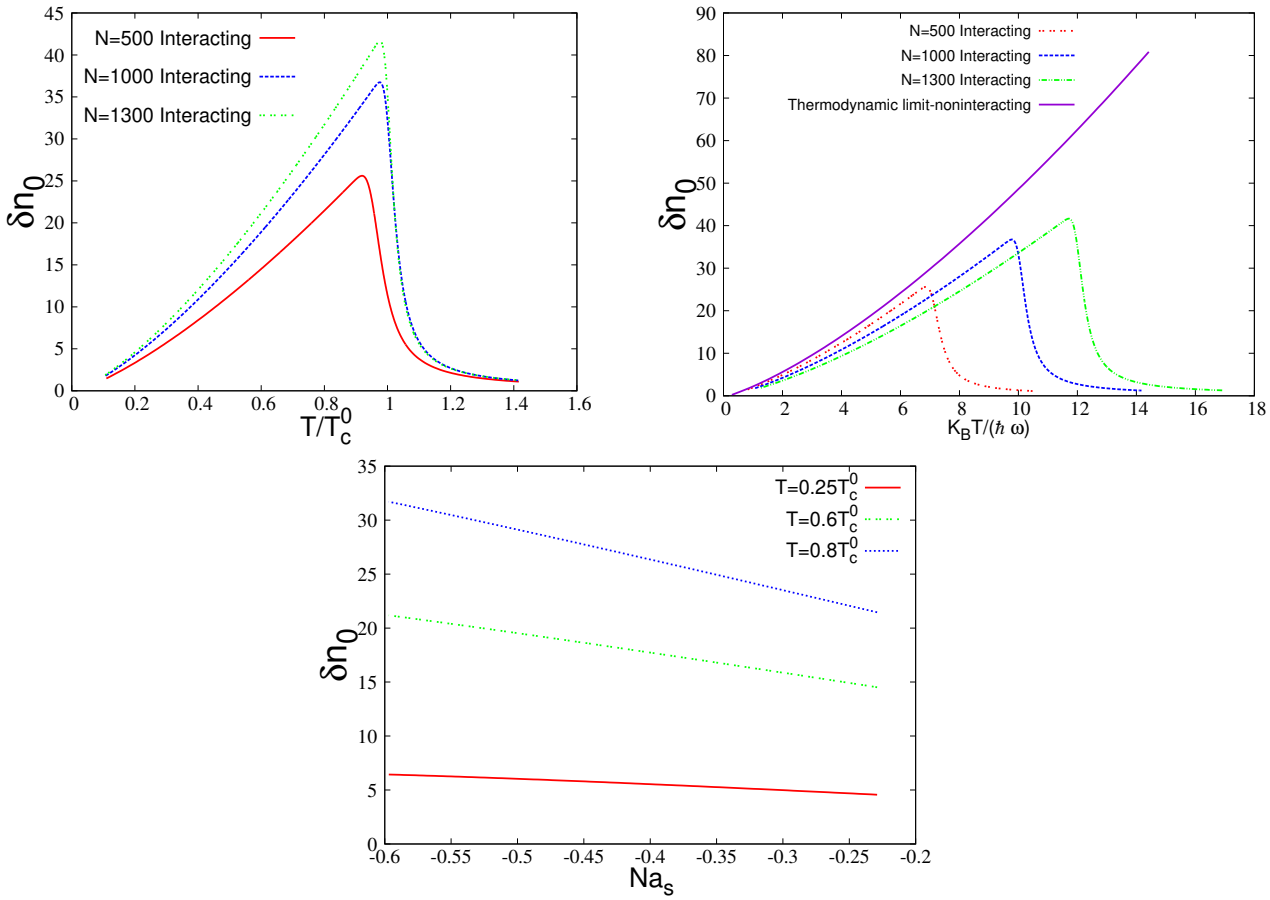

FIG. 4. (Color online) Plot of δn_0 with respect to reduced temperature $\frac{T}{T_c^0}$ [Figure 3(a) and 3(b)] and with $\frac{k_B T}{\hbar\omega}$ [Figure 3(c)] and also with Na_s for interacting and noninteracting atoms of ^7Li and ^{87}Rb in the harmonic and anharmonic trap.

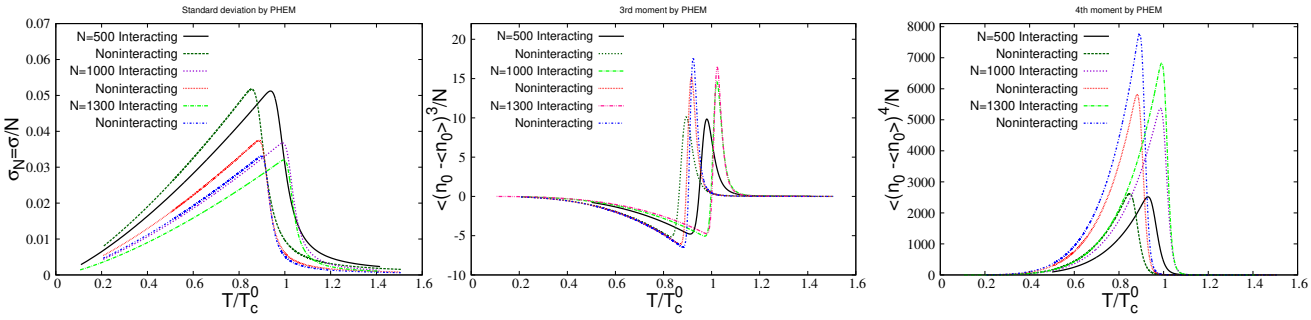

FIG. 5. Second-, third- and fourth- order of central moments for ^7Li condensate

where $\gamma = 0.57722$ is Euler's constant and $\zeta(2)$ is the Riemann Zeta functions. Thus Figure 4(b) nicely exhibits that at large particle limit the fluctuations are expected to have desired behaviour. The curves exhibit a maxima at a particular temperature and then drops to zero sharply. At much lower temperature the fluctuations are independent of particle number. However unlike our previous observation for repulsive BEC [**?**], for attractive BEC we observe the dependence of N in the moderate temperature well below to achieve maxima. At higher temperature all the graphs sharply fall to zero as expected. In Figure 4(c), we plot δn_0 as a function of Na_s for the above reported set of temperatures. Thus we observed that the effect of attractive interaction enhances the condensation process significantly.

In Fig. 5 and 6 we plot the several fluctuations quantities for attractive and repulsive BEC with harmonic as well as in anharmonic trap. The general trend remains same for both cases, however the finite size effect is seen in the

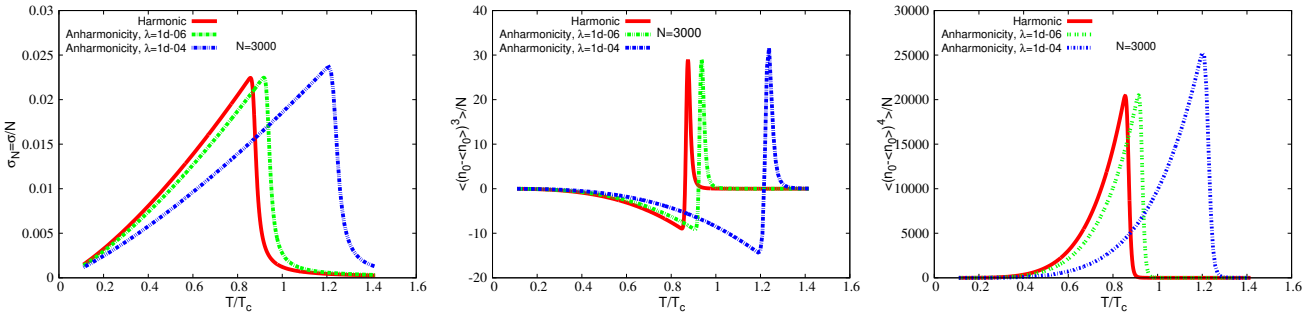

FIG. 6. Second-, third- and fourth- order of central moments for ^{87}Rb condensate

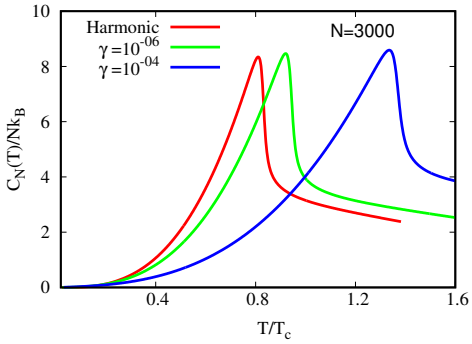

FIG. 7. Plot of specific heat of interacting bosons both in anharmonic and harmonic trap with $N = 1000$.

curvature. For smaller particle number, we observe very broad maxima at the transition point, whereas for larger particle the sharpness increases. Of course it supports the true phase transition in thermodynamic limit, but not for mesoscopic condensate. We do not find any possibility of phase transition in anharmonic trap, although it favours achievement of BEC at higher temperature.

A true phase transition is signalled by a singularity in thermodynamic potential [1]. A finite discontinuity in the first derivative of the thermodynamic potentials is usually termed as first-order phase transition. Whereas if the first derivatives are continuous but second derivatives are discontinuous, the transition is categorized as the higher-order. To know whether there is true phase transition or not I have studied the thermodynamical quantity specific heat(C_v) for anharmonic trap. Figure 7 shows the variation of C_v with anharmonic trap. Though for tight trap the nature of C_v around T_C is sharp but we could not relate it with a true phase transition for our mesoscopic BEC. With every phase transition a critical exponent can be defined but for the quasi-phase transition we will call it transition exponent (λ_c). It can be calculated by the following prescription: The critical exponent for any thermodynamic function is usually defined as

$$\lambda_c = \lim_{t\to 0} \frac{\ln|F(t)|}{\ln|t|}, \tag{49}$$

where t is the reduced temperature $t = \frac{T-T_C}{T_C}$ or it can be written as $F(t) \sim t^{\lambda_c}$, it basically represent the asymptotic behaviour of the thermodynamic function at $t \to 0$. Thus at the critical temperature $F(t)$ either vanishes or be singular. However for mesoscopic BEC, as $C_N(T)$ becomes sharper smoothly with increase in particle number N, neither vanishes nor become singular. Instead we follow the following prescription [].

$$F(t) = F(0) + b|t|^{\lambda_1} + ..., \tag{50}$$

as λ is zero, λ_1 is the leading exponent.

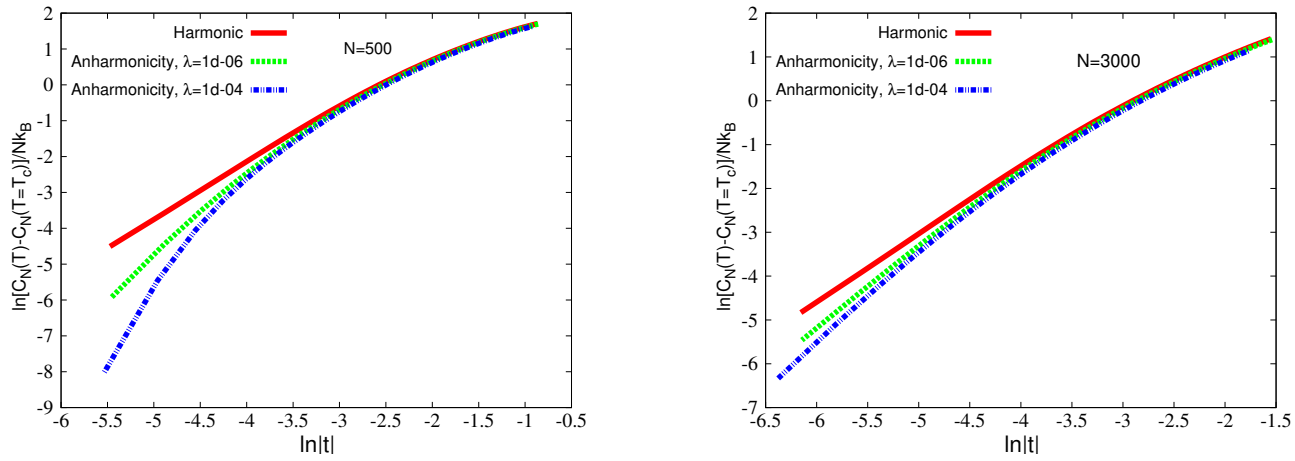

FIG. 8. Exponent curves for the ^{87}Rb atoms with N=500 in [panel(a)] and N=3000 in [panel(b)] both in harmonic and anharmonic trap.

We define λ_1 as the transition exponent

$$\lambda_1 = \lim_{t\to 0} \frac{\ln|F(t) - F(0)|}{\ln|t|}, \tag{51}$$

In Figure 8(a) and 8(b) we plot $\ln[\frac{C_N(T)-C_N(T=T_C)}{Nk_B}]$ as a function of $\ln|t|$ for $N = 500$ and 3000. Each graph reports both cases of anharmonicity together with harmonic trap. The appropriate difference between harmonic trap and anharmonic trap exists. We fit a straightline which calculates the exponent 1.798 for $\lambda = 10^{-6}$ and 1.826 for $\lambda = 10^{-4}$.

Publications regarding this results::

1.**Statistical properties and condensate fluctuation of attractive Bose gas with finite number of particles**Sangita Bera, Mantile Leslie Lekala, Barnali Chakrabarti, Satadal Bhattacharyya , Gaotsiwe Joel Rampho [**Physica A 481 (79-89),2017.**]
2. **Mesoscopic Bose-Einstein condensate in anharmonic trap: concept of transition exponent** M. L. Lekala, S. Bera, G. J. Rampho, B. Chakrabarti, S. Bhattacharyya [**accepted in Few Body Problems in Physics (2018)**]
3. **Does the statistical fluctuations of mesoscopic Bose-Einstein condensation exhibit self-similar dependence on trap shape ?** S. Bera · M. L. Lekala · G. J. Rampho · B. Chakrabarti · S. Bhattacharyya [**Submitted in the jour. Low.Temp. Phys.**]

B. Result for strongly interacting and highly correlated BEC

1. *Sorting Fermionization from Crystallization in Many-Boson Wavefunctions*

We first independently characterize fermionization and crystallization from a many-body point of view respectively. Thereafter, we investigate how to sort the one, fermionization, from the other, crystallization. Bosons fermionize when they feel an infinitely repulsive contact interaction in one spatial dimension. For fermionized bosons, the total energy E and the density [Eq. (39)] of the system become exactly equal to the energy and the density of non-interacting spinless fermions, respectively. For our showcase of $N = 4$ bosons in a harmonic trap with frequency one, $V(x) = \frac{1}{2}x^2$, the limiting value is thus $E^{N=4}_{\lambda\to\infty} = 8$. We start our investigation with the one-body density as a function of interaction strength λ [Fig. 9(a-b)]. For comparatively weak repulsion $\lambda < 10$, the density is clustered at the center of the trap, but becomes flatter and broader when λ increases. For stronger repulsion, the density gradually acquires modulations and the number of humps finally saturates to the number of bosons in the system; four humps are clearly visible when the interaction strength goes above $\lambda \sim 10$. The emergence of N maxima in the density indicates that the TG regime is approached. The density humps are more pronounced in the center of the trap, where the potential is close to zero. For larger distances from the origin, the humps in the density are less pronounced due to the non-zero value of the confinement potential. Importantly, the density modulations also become less pronounced

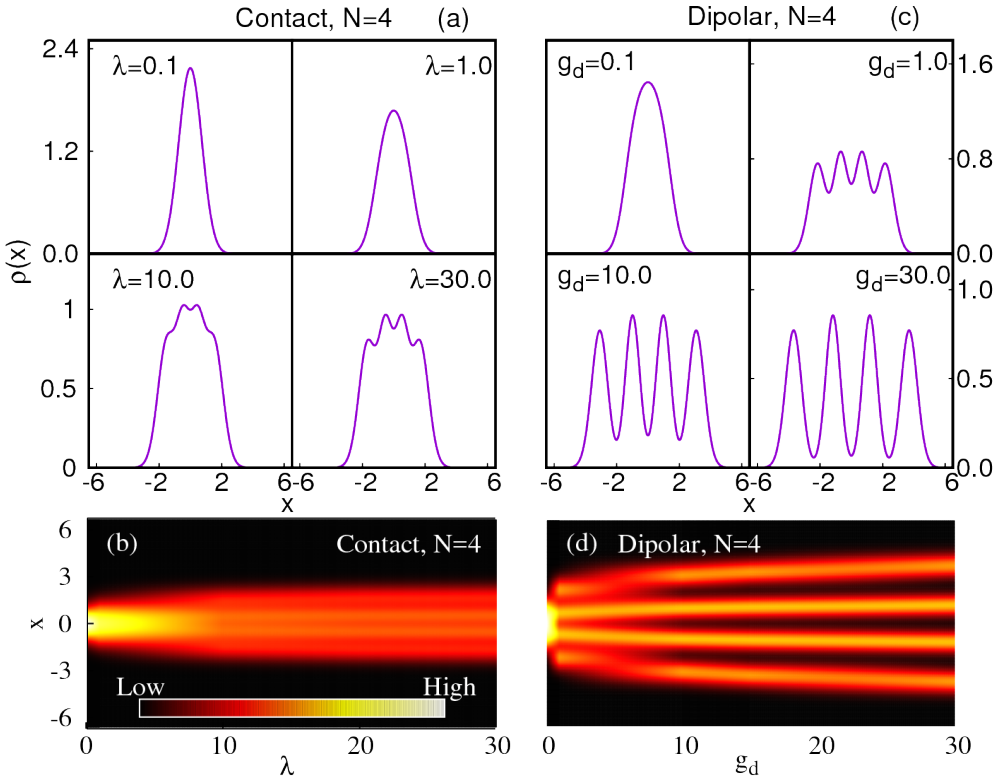

FIG. 9. One-body density of four bosons as a function of contact [(a),(b)] and dipolar [(c),(d)] interparticle interaction strength.

if the number of particles N is increased. We note that the density's maxima in this Tonks regime are distinct but *not isolated*. We also observe that the density does not broaden further, once the TG regime has been reached.

We now move to discuss the two-body densities $\rho^{(2)}$ of bosons with contact interactions [see Fig. 10(a)]. For weak interaction strength, $\lambda = 0.1$, the bosons are clustered near the center, i.e, $x_1 = x_2 = 0$. As the interaction strength increases, $\rho^{(2)}$ spreads out to the off-diagonal ($x_1 \neq x_2$) while the diagonal ($x_1 \sim x_2$) is depleted (for $\lambda = 1$). For stronger repulsion a so-called "correlation hole" in the two-body density forms on the diagonal, $\rho^{(2)}(x, x) \to 0$ [for $\lambda = 10$ and $\lambda = 30$]. The probability of finding two bosons at the same position tends towards zero. In the limit of infinite repulsion the correlation hole persists in $\rho^{(2)}$. In analogy, however, to the boundedness of the energy as a function of the interaction strength, the width of two-body density on its anti-diagonal $[\rho^{(2)}(x, -x)]$ is also bounded, i.e., the spread of $\rho^{(2)}$ converges in the fermionization limit when $\lambda \to \infty$. Similar to the one-body density, the maxima which are formed in the off-diagonal of the two-body density are distinct but not isolated [see Fig. 10(a) for $\lambda = 10$ and $\lambda = 30$]. We infer that *the correlation hole along the diagonal* and *the confined spread* are the unique signatures of the two-body density of a fermionized state.

For bosons with dipole-dipole interactions, crystallization occurs when the long-range tail of the interaction [see Eq. (35)] becomes dominant [**?**]: the bosons form a lattice structure which allows them to minimize their mutual overlap. To characterize crystallization we analyze the one-body and two-body density for bosons with dipolar interaction of strength g_d. We choose the cut-off parameter $\alpha_0 = 0.05$ in Eq. (35) such that the effective interaction $V_{eff} = \int_{-10.0}^{10.0} \frac{g_d}{x^3+\alpha} dx = \int_{-10.0}^{10.0} \delta(x) dx = 1.0$. We plot the one-body density of $N = 4$ bosons as a function of g_d in Fig. 9(c) and (d). The system is condensed at the center of the trap for small g_d. As g_d increases, the density starts to exhibit a four-hump structure (see Fig. 9(c) and (d) for $g_d \in [\sim 1, \sim 5]$) similar to the density observed for the fermionization of bosons with contact interactions [Fig. 9(a)].

We now analyze the two-body density for dipole-dipole interactions [Fig. 10(b)]. For small interaction strength, $g_d = 0.1$, the atoms are clustered together at the center of the trap. As g_d increases, a correlation hole develops: $\rho^{(2)}(x, x)$ tends to zero [Fig. 10(b) for $g_d \geq 1$]. Thus, due to the long-range interaction, the probability of finding two bosons in the same place is strongly reduced. In the crystalline phase [Fig. 10(b) for $g_d \geq 10$]: the bosons escape their spatial overlap entirely and even the off-diagonal peaks of $\rho^{(2)}$ become isolated. We term this behavior the formation

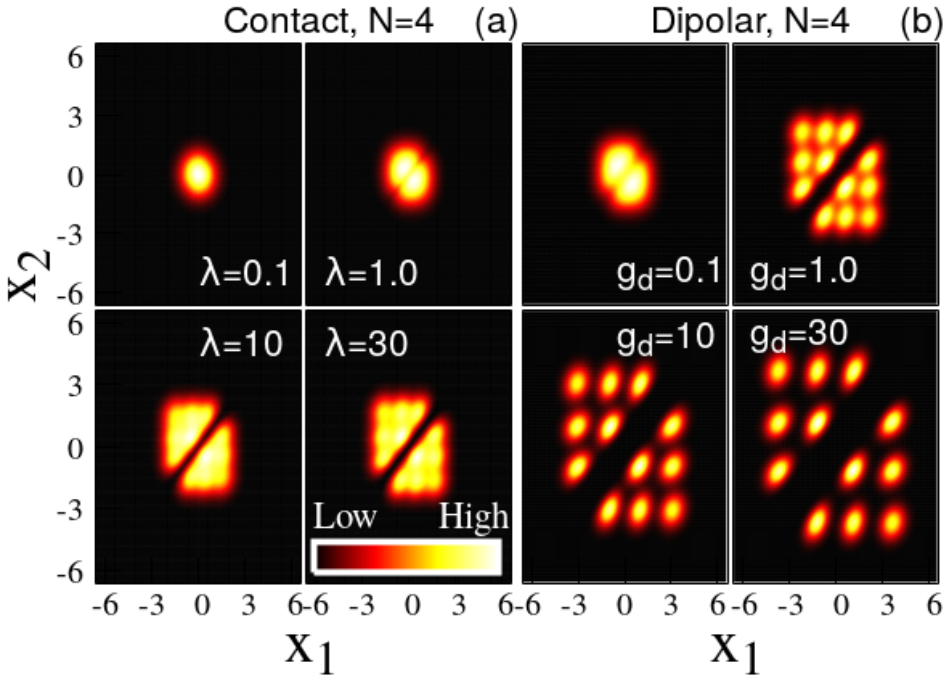

FIG. 10. Two-body density of four bosons as a function of contact (a) and dipolar [(b)] interparticle interaction strength.

of an off-diagonal correlation hole. For crystallized bosons, the spread of the anti-diagonal of the two-body density, $\rho^{(2)}(x,-x)$, is diverging as g_d is increasing [compare Fig. 10(b) for $g_d = 10$ to Fig. 10(b) for $g_d = 30$].

We assert that *the correlation hole along the diagonal and the off-diagonal* and *the unbounded spreading* are the unique signatures of the two-body density of a crystalline state of dipolar bosons. We quantify the spreading of the density as a function of interactions and plot the position of its outermost peak as a function of the interaction strength in Fig. 11(a) and compare it to the energy in Fig. 11(b). The bounded spreading of the density for contact interactions is a consequence of the bounded energy as the interaction strength tends to infinity. Similarly, the unbounded spreading of the density for dipole-dipole interactions is a consequence of the unbounded energy as the interaction strength g_d tends to infinity. The natural occupations for several orbitals both for contact and dipolar interactions are shown in Fig. 11(c) and Fig. 11(d).

2. Study of entropies for relaxation process

We now present numerical results for different kinds of Shannon information entropy for contact interaction and different orders of long range interactions (LRI). Our main motivation is to make a connection of the transition to the chaotic to thermalization regime through entropy production. In Fig. 12 (top panel of left figure), we plot S^{info} for contact interaction, while in the bottom panel we plot it for different LRI (for different values of α's). The GOE value of S^{info} for our system is 5.40. This GOE value is calculated as $S^{info}_{GOE} = \ln 0.48D$ where D is the length of the Hilbert space and can be written as $D = \begin{pmatrix} N+M-1 \\ N \end{pmatrix}$. We observe that in all cases S^{info} is very close to zero for weak interactions when a single coefficient mostly contributes. Increasing the interaction strength, as delocalization starts, S^{info} increases. However for LRI delocalization happens in a faster way, and we observe sharp increase followed by saturation to GOE value. Notice, anyway for contact interaction the numerical value of saturation is below the GOE limit.

Fig. 12(right) reports the same as in Fig. 12(left) but for the occupation entropy S^{occu} for weak interaction S^{occu} is close to zero. Increasing the interaction strength, other natural orbitals are occupied until S^{occu} saturates to GOE value. D is set equal to the number of orbitals M in the MCTDHB for occupation entropy and $S^{occu}_{GOE} = -\sum_{i=1}^{M}\left(\frac{1}{M} ln \frac{1}{M}\right) = ln(M)$ Note that the GOE limit of S^{occu} is 1.79.

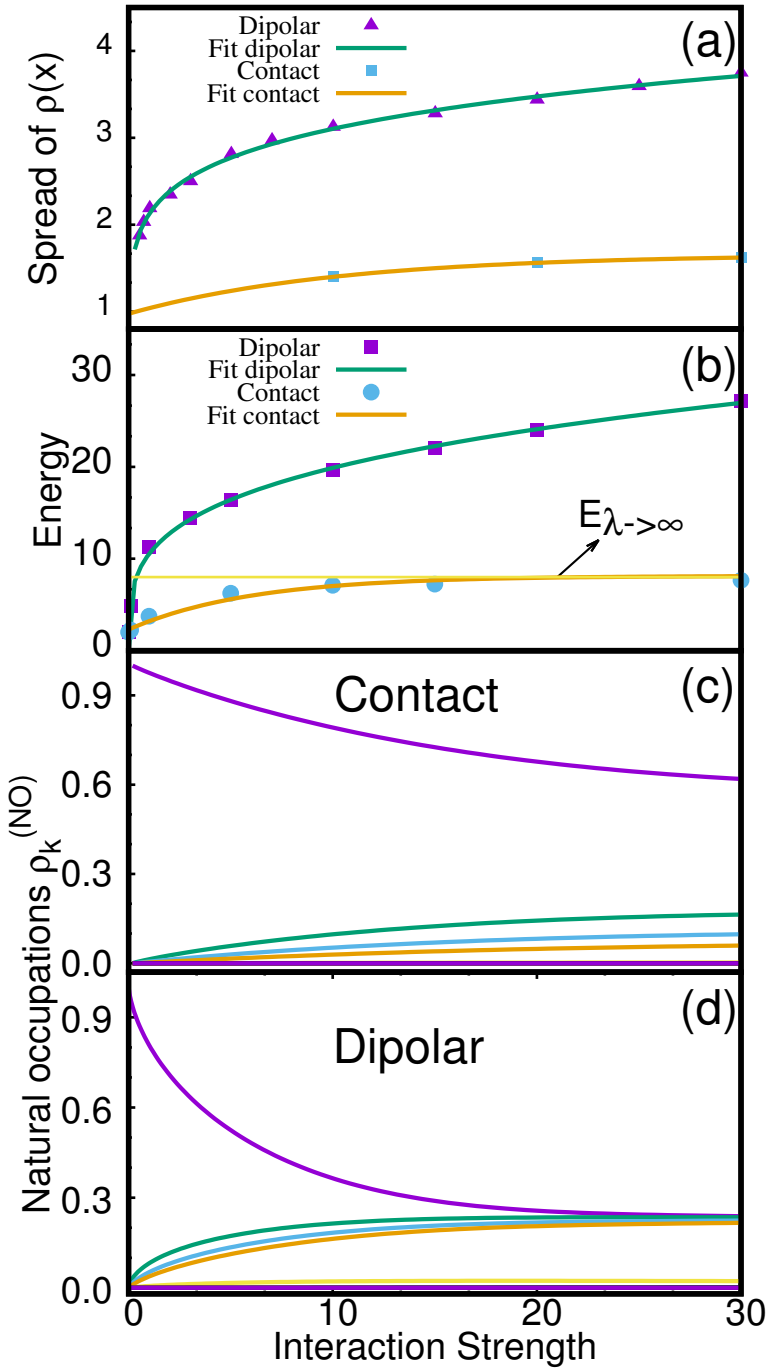

FIG. 11. Tracing fermionization and crystallization in the spread of the density (a), the energy (b), and the natural occupations (c),(d) as a function of the interaction strength.

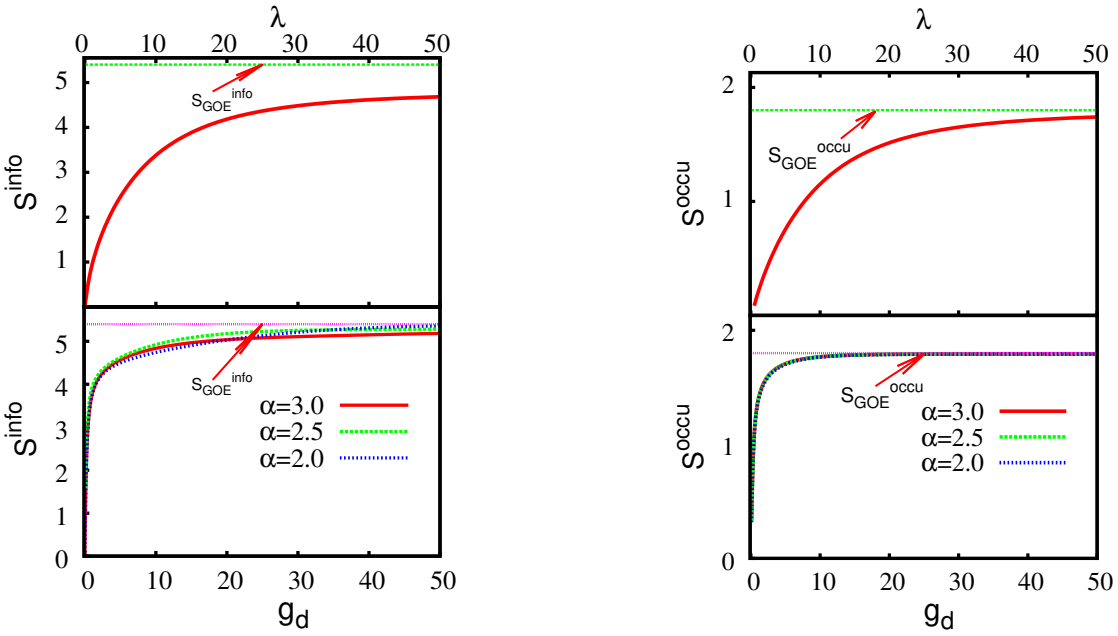

FIG. 12. Shannon information entropy S^{info} and Occupation entropy: Top panel for contact interaction, bottom panel for several LRI

In Fig. 13 we plot the absolute value of the normalized first-order correlation function, $|g^{(1)}(x',x)|^2$, with the left column corresponding to contact interaction and the right one to LRI with $\alpha = 3.0$. In general passing from localization to delocalization can be characterized by the clear signature of loss of coherence. However noticeable difference exists between the LRI and the contact interaction. For weak interaction, such as $\lambda = 0.1$, the first-order coherence is present throughout the trap for contact interaction, while in the case of LRI we can distinguish the diagonal correlations from the off-diagonal correlations. This is the effect of long-range tail in the LRI. Gradually, increasing the interaction strength, the off-diagonal correlation is lost and diagonal correlation is at variance maintained. However the vanishing of the off-diagonal correlation occurs for smaller interaction strength in the case of LRI. Our simulation for other values of α show similar results, only the loss of off-diagonal coherence is faster when the value of α is decreased.

In Fig. 14 we plot the two-body correlation function $g^{(2)}(x,x')$ for the same parameters as reported in Fig. 13. We observe that $g^{(2)}(x,x') \simeq 1$ for almost all x', x, although we observe local decrease in the second-order coherence for contact interaction. $g^{(2)}$ is maximal along the diagonal for contact interaction showing the maximum probability of detecting two particles for all $x \simeq x'$. Whereas increasing the interaction strength, coherence is maintained at the off-diagonal but not on the diagonal. The vanishing diagonal part of the normalized two-body correlation function is called the anti-bunching effect, as clearly seen for dipolar LRI. The reason is that due to the long-range repulsion, the probability of finding a double occupation along the diagonal is practically zero.

3. Relaxation dynamics of 1D-Bose gas in optical lattice

In my research work, I have simulated the quench dynamics of one-dimensional Bose gas in a triple well ($S = 3$) optical lattice for $N = 3$ particles. We direct a superfluid (SF) to Mott-insulator (M I) transition by performing two independent processes: an interaction quench induced transition and a lattice depth quench induced transition. The Shannon information entropy for interaction quench as a function of time is shown in Fig. 15 and Fig. 16(a). It is very clear from Fig. 15 that there is only periodic oscillation in time for $S(t)$. We observe a generic linear increase at a shorter time followed by saturation for large interaction strength (Inset of Fig. 16(a)). The sharp linear increase in $S(t)$ is attributed to an exponential increase in the time-dependent natural occupation contributing to the dynamics. Reference [33] showed that when the two-body interaction is completely random, the quench dynamics can

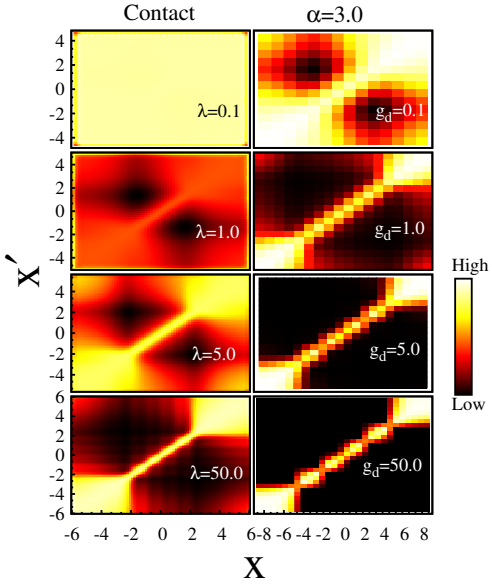

FIG. 13. The normalized first-order correlation function $|g^{(1)}(x,x')|^2$ is plotted for several interaction strengths for 1D Bose gas in harmonic trap.. Left column corresponds to the contact interaction, whereas right column corresponds to dipolar interaction.

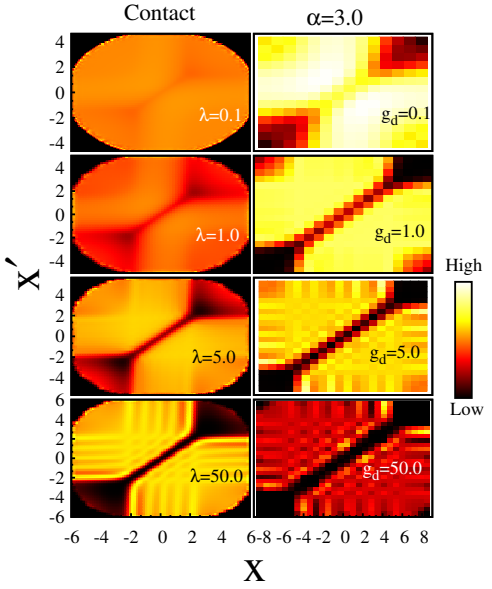

FIG. 14. The normalized second-order correlation function $|g^{(2)}(x,x')|$ for several interaction strengths for 1D Bose gas in harmonic trap. Left column corresponds to the contact interaction and the right column corresponds to the dipolar interaction.

be described analytically, the linear increase in $S(t)$ is described by

$$S(t) = \Gamma\ t\ \ln P \tag{52}$$

where Γ is determined by the decay probability to stay in the initial ground state and P is the number of many-body states involving in the dynamics. Although in our dynamical model, there is no randomness *ab initio*, we observe that when the interaction strength is very strong (exceeds some critical value) the analytic expression of reference [33] works well. The saturation of $S(t)$ happens due to the complete occupation of the available finite sized Hilbert space. For Gaussian orthogonal ensemble (GOE) of random matrices the saturation value of information entropy is given by $S_{GOE} = -\sum_{i=1}^{M}(\frac{1}{M})\ln(\frac{1}{M}) = \ln(M)$, where M is the number of orbitals [**? ? ?**]. For $M = 18$ orbital the GOE

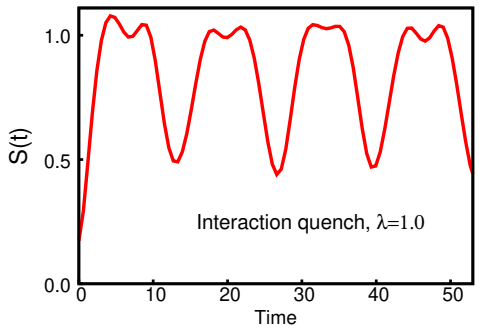

FIG. 15. Dynamics of Shannon entropy $S(t)$ for interaction quench $\lambda = 1.0$. The entropy shows periodic oscillation. All the quantities are dimensionless.

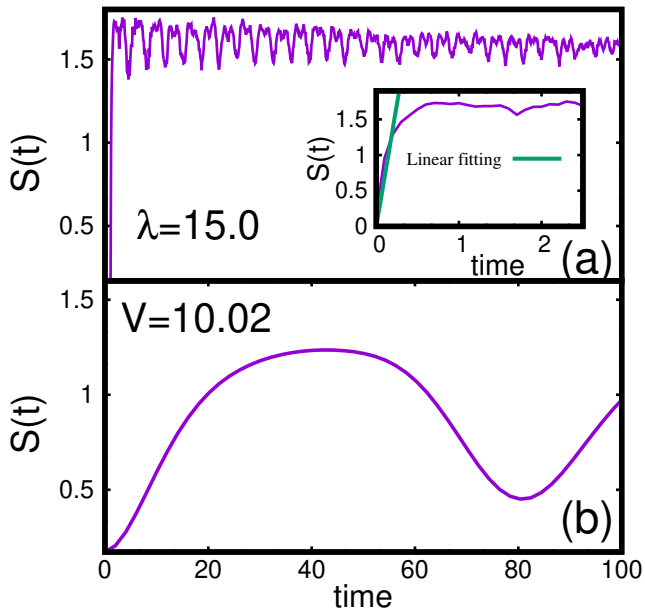

FIG. 16. Panel(a) Dynamics of Shannon entropy $S(t)$ for interaction quench $\lambda = 15.0$. The sharp linear increase followed by saturation signify that the system relaxes to the maximum entropy state. The saturation value is = 1.62. Panel(b) Dynamics of Shannon entropy $S(t)$ for lattice-depth quench $V = 10.02$. The entropy exhibits periodic oscillation and the possibility of relaxation is ruled out. All the quantities are dimensionless.

prediction $S_{GOE} = 2.89$. The saturation value of Shannon entropy for our present simulation is $S^{sat} = 1.62$. This value of saturation is below the GOE value as we are dealing with finite interaction. However, the system relaxes to the maximum entropy state.

The corresponding Shannon entropy for lattice depth quench as shown in Fig. 16(b), also exhibits the periodic oscillation in time. The absence of a generic linear increase and saturation guarantees that the system will not relax. To check the possibility of relaxation for very strong lattice depth quench, we repeat the simulation for very strong quench when the system is pumped with huge energy. But we do not find any signature of relaxation, only the revival time decreases.

Publications regarding this results ::

1. **Sorting Fermionization from Crystallization in Many-Boson Wavefunctions.** S. Bera, B. Chakrabarti, A. Gammal, M. C. Tsatsos, M. L. Lekala, B. Chatterjee, C. Lévêque, and A. U. J. Lode. **arXiv:1806.02539**

[cond-mat.quant-gas]; Under review in the journal Phys. Rev. A
2.**Chaos vs Thermalization for bosonic systems with power-law interactions.** S. Bera, B. Chakrabarti, A. Trombettoni, M. L. Lekala, and G. J. Rampho. **Under review in the jounal Phys. Rev. E**
3.**Probing relaxation dynamics of strongly correlated 1D Bose gas in optical lattice.** S. Bera, R. Roy, A. Gammal, B. Chakrabarti, and B. Chatterjee. **arXiv:1807.09003 [cond-mat.quant-gas]; Submitted after minor corrections in the journal Phys. Rev. A**

---

[1] M. H. Anderson, J. R. Ensher, M. R. Matthews, C. E. Wieman, and E. A. Cornell, Science **269**, 198 (1995); K. B. Davis, M. C. Mewes, M. R. Andrews, N. J. van Druten, D. S. Durfee, D. M. Kurn, and W. Ketterle, Phys. Rev. Lett. **75**, 3969 (1995).
[2] J. R. Ensher, D. S. Jin, M. R. Matthews, C. E. Wieman, and E. A. Cornell, Phys. Rev. Lett. **77**, 4984 (1996).
[3] C. C. Bradley, C. A. Sackett, and R. G. Hulet, Phys. Rev. Lett. **78**, 985 (1997).
[4] Cornish, S. L., Claussen, N. R., Roberts, J. L., Cornell,E. A., and Wieman, C. E., Phys. Rev. Lett., **2000**, 85, 1795.
[5] F. Dalfovo, S. Stringari, *Phys. Rev. A* **53**, 2477 (1996).
[6] C. J. Pethick and H. Smith, *Bose-Einstein Condensation in Dilute Gases* (Cambridge University Press, Cambridge UK, 2002).
[7] E. P. Gross, N. Cemento **20**,454,(1961), J. Math. Phys. 4, 195 (1963).
[8] L. P. Pitaevskii, ZH. Eksp. Teor. Fiz. **40**, 646 (1961).
[9] D. Blume and C. H. Green Phys Rev A 63, 063601 (2001).
[10] J. L. DuBois and H. R. Glyde Phys Rev A 68, 033602, (2003).
[11] D. M. Caperley and B. J. Alder Phys. Rev. Lett **45**, 566, (1980).
[12] J. L. DuBois and H. R. Glyde Phys Rev A 63, 023602, (2001).
[13] L. Pitaevskii and S. Stringari, Bose-Einstein Condensation (Clarendon, Oxford, 2003); S. Giorgini, L. P. Pitaevskii, and S. Stringari, Phys. Rev. Lett. 80, 5040 (1998).
[14] V. V. Kocharovsky et al., Adv. At. Mol. Opt. Phys. 53, 291 (2006); V. V. Kocharovsky, Vl. V. Kocharovsky, and M. O. Scully, Phys. Rev. Lett. 84, 2306 (2000).
[15] S. Grossmann and M. Holthaus, Phys. Rev. Lett. 79, 3557 (1997); M. Holthaus and E. Kalinowski, Ann. Phys. (N.Y.) 276, 321 (1999).
[16] Ballot, J. L., and Fabre de la Ripelle, M., Ann. Phys. (NY), 1980, 127, 62.
[17] M. Fabre de la Ripelle, *Few-Body Syst.* **1**, 181 (1986).
[18] A. Svidzinsky and M. Scully, Phys. Rev. A 82, 063630 (2010); K. E. Dorfman, M. Kim, and A. A. Svidzinsky, ibid. 83, 033609 (2011).
[19] K. Huang, Statistical Mechanics, 2nd ed. (Wiley, New York, 1987).
[20] S. Bhattacharyya, T. K. Das, and B. Chakrabarti, Phys. Rev. A 88, 053614 (2013).
[21] T. K. Das and B. Chakrabarti, Phys. Rev. A 70, 063601 (2004).
[22] T. K. Das, S. Canuto, A. Kundu, and B. Chakrabarti, Phys. Rev. A 75, 042705 (2007).
[23] S. Goswami, T. K. Das, and A. Biswas, Phys. Rev. A 84, 053617 (2011); A. Biswas, J. Phys. B 42, 215302 (2009).
[24] Ofir E. Alon, Alexej I. Streltsov, and Lorenz S. Cederbaum, Phys. Rev. A **77**, 033613 (2008).
[25] A. I. Streltsov, O. E. Alon, and L. S. Cederbaum, Phys. Rev. Lett. **99**, 030402 (2007).
[26] A. U. J. Lode, M. C. Tsatsos, E. Fasshauer, R. Lin, L. Papariello, P. Molignini, and C. Lévêque, MCTDH-X: *The time-dependent multiconfigurational Hartree for indistinguishable particles software*, http://ultracold.org (2018).
[27] A. U. J. Lode, *Tunneling Dynamics in Open Ultracold Bosonic Systems*, Springer Theses, (Springer, Heidelberg, 2014).
[28] A. U. J. Lode, Phys. Rev. A **93**, 063601 (2016).
[29] E. Fasshauer and A. U. J. Lode, Phys. Rev. A **93**, 033635 (2016).
[30] *Geometry of the time-dependent variational principle*, P. Kramer and M. Saracen, (Springer, Berlin, 1981).
[31] A. U. J. Lode, B. Chakrabarti, and V. K. B. Kota, *Phys. Rev. A* **92**, 033622 (2015).
[32] O. Penrose and L. Onsager, Phys. Rev. **104**, 576 (1956).
[33] V. V. Flambaum and F. M. Izrailev, Phys. Rev. E **64**, 036220 (2001).
[34] B. Chakrabarti, T.K. Das, P.K. Debnath, J. Low Temp. Phys. **157** 527–540 (2009).
[35] A. Biswas, T.K. Das, L. Salasnich, B. Chakrabarti, Phys. Rev. A **82** 043607 (2010).
[36] T. K. das and B. Chakrabarti, *Phys. Rev. A* **70**, 063601 (2004).
[37] T. K. Das, S. Canuto, A. Kundu and Barnali Chakrabarti *Phys. Rev. A* **78**, 042705 (2007).
[38] S. A. Sofianos, *et al.*, *Phys. Rev. A* **87**, 013608 (2013).
[39] Chakrabarti, B., and Das, T. K., Phys. Rev. A, **78**, 063608 2008.
[40] Das, T. K., Coelho, H. T., and Fabre de la Ripelle, M., Phys. Rev. C, **1982**, 26, 2281.
[41] E. Ö. Karabulut, M. Koyuncu and M. Tomak Physica A **389**, 1371, (2010).
[42] M. Abramowitz and I. A. Stegun, *Handbook of mathematical functions, National Institute of Standards and Technology, USA (1964).*
[43] T. Landsberg, *Thermodynamics with Quantum Statistical Illustration* (Interscience, New York, 1961).
[44] E. D. Trifonov and S. N. Zagoulaev, *Physics-Uspekhi* **53(1)** (83-90) (2010).

[45] N.L. Balazs and T. Bergeman, *Phys. Rev. A* **58**, 2359 (1998).
[46] We divide the dimensional Hamiltonian by $\hbar^2/(mL^2)$, where m is the mass of the considered bosons and L a conveniently chosen length scale.
[47] M. Olshanii, Phys. Rev. Lett. **81**, 938 (1998).
[48] R. J. Glauber, *Phys. Rev.* **130**, 2529 (1963).